Advanced Ceramics Progress: Vol. 11, No. 1, (Winter 2025) 36-46

Materials and Energy Research Center
MERC

Contents lists available at ACERP

Advanced Ceramics Progress

Journal Homepage: www.acerp.ir

Original Research Article

Effect of Current Density on Microstructure, Mechanical, and Corrosion Behavior of Ni-P-TiO_2 Composite Coating

Mina Afzali Gorouh [a], Hadi Ebrahimifar [b,*], Farhad Mohsenifar [c]

[a] *MSc Graduate, Department of Materials Engineering and Metallurgy, Faculty of Engineering, Shahid Bahonar University of Kerman, Kerman, Iran.*

[b] *Associate Professor, Department of Materials Engineering, Faculty of Mechanical and Materials Engineering, Graduate University of Advanced Technology, Kerman, Iran.*

[c] *Assistant Professor, Mechanical Engineering Department, Faculty of Engineering, Higher Education Complex of Bam, Bam, Kerman, Iran.*

* Corresponding Author Email: H.ebrahimifar@kgut.ac.ir (H. ebrahimifar) URL: https://www.acerp.ir/article_232183.html

ARTICLE INFO

Article History:
Received 21 July 2025
Received in revised form 25 August 2025
Accepted 07 October 2025

Keywords:
Electroplating,
Ni-P-TiO_2 Coating,
Wear Resistance,
Corrosion

ABSTRACT

Coatings are extensively applied in various industries due to their notable hardness, corrosion resistance, and superior mechanical and chemical properties. One method to enhance their wear resistance is the incorporation of oxide particles, such as TiO_2. In this work, a Ni-P-TiO_2 composite coating was synthesized through electroplating, and the influence of current density during electrodeposition on the microstructure and tribological properties was examined. Coating morphology was investigated using scanning electron microscopy (SEM), while phase composition and crystallite size were determined by X-ray diffraction (XRD) analysis. The microhardness of the samples was measured using a Vickers microhardness apparatus. A pin-on-disc test was employed to evaluate the wear resistance of coated and uncoated samples. Furthermore, corrosion behavior was assessed through potentiodynamic polarization and electrochemical impedance spectroscopy (EIS) measurements in a 3.5% NaCl solution. Results demonstrated that lowering the current density leads to finer crystallites, decreased microhardness, and reduced wear resistance. Potentiodynamic polarization and EIS tests revealed that increasing the electroplating current density diminishes the corrosion resistance of the coatings.

https://doi.org/10.30501/acp.2025.536027.1180

1. INTRODUCTION

Ferritic stainless steels are chromium–iron alloys characterized by a body-centered cubic (BCC) crystal structure, typically containing between 10.5 and 30% chromium. Chromium plays a critical role as an alloying element, not only in enhancing corrosion resistance but also in improving the heat resistance of steels (Sun et al., 2022). These steels are widely used in industry, and to further enhance their resistance to wear, oxidation, and corrosion, protective coatings are often employed. Nickel-based coatings are among the most widely used for this purpose; however, pure nickel does not sufficiently provide all the required functional properties. Consequently, nickel-phosphorus (Ni-P) and composite coatings are frequently adopted. Ni-P coatings exhibit superior hardness, significant wear resistance, and enhanced corrosion protection (Fukunaga & Ueda, 2024; Shozib et al., 2021). In these coatings, increasing phosphorus content improves corrosion resistance while reducing hardness and wear resistance (Yongfeng et al., 2017). The characteristics of electroplated coatings are influenced by multiple process parameters. Key factors include the concentration of particles in the plating bath, the applied current density, and the electrolyte pH, all of

Please cite this article as: Afzali Gorouh, M., Ebrahimifar, H. & Mohsenifar, F. (2025). Effect of Current Density on Microstructure, Mechanical, and Corrosion Behavior of Ni-P-TiO_2 Composite Coating, *Advanced Ceramics Progress*, 11(1), 36-46. https://doi.org/10.30501/acp.2025.536027.1180

which play a decisive role in determining the concentration of deposited particles in the coating, the crystallite size, and the mechanical properties of the coating (Rai & Gupta, 2021). Other parameters, such as bath temperature, plating time, stirring speed, and the incorporation of various additives, also significantly affect coating quality (Mohsenifar et al., 2024). Owing to the advantages of electroplating, namely, its low cost, ease of process control, and high deposition rate, this study employed a nickel sulfate bath under direct current conditions, facilitating the formation of nickel coatings with low internal stresses and satisfactory toughness (Rudnik, 2024).

Previous research has reported the development of Ni-based composite coatings reinforced with particles such as TiO_2, Al_2O_3, SiC, CeO_2, and Fe_2O_3 to enhance the performance of conventional Ni coatings (Karthik et al., 2020; Ma et al., 2024; Zhang et al., 2021). The incorporation of these reinforcement phases has been shown to significantly improve the mechanical strength, tribological behavior, and corrosion and oxidation resistance of the coatings. The final performance of such composites, however, is largely governed by factors including crystallite size, the distribution of reinforcing particles, and various electroplating parameters. The optimization of electroplating parameters, particularly current density, plays a crucial role in achieving uniform particle distribution, controlling particle co-deposition within the metallic matrix, and thereby determining the overall performance of composite coatings.

Numerous studies have examined the influence of current density on the incorporation of reinforcing particles into the Ni-P matrix, though the reported outcomes vary. For example, while some investigations demonstrated a direct correlation between current density and the co-deposition of SiC particles in Ni-P coatings, others identified an inverse relationship (Chou et al., 2005; Hansal et al., 2013). Lekmine (Lekmine et al., 2022) reported that increasing current density enhanced the incorporation of TiO_2 particles in Ni-P-TiO_2 coatings deposited on copper substrates. Sadeghi (2016) investigated the influence of various reinforcing particles on the properties of Ni-P coatings and reported that, under identical working conditions, TiO_2 particles were more effective than SiC and Al_2O_3 in reducing internal stresses and enhancing the structural integrity of the coating. Similarly, Saravanan et al. (2020) demonstrated that the incorporation of TiO_2 into the electroless bath improves the wear resistance of Ni-P-TiO_2 composite coatings. Chen et al. (2010) showed that combining electroless plating with the sol-gel technique enables a more uniform dispersion of TiO_2 particles within the Ni-P matrix. The resulting composite coating exhibited superior hardness and wear resistance relative to conventional Ni coatings. Yongfeng et al. (2017) confirmed the beneficial role of TiO_2 particles in enhancing the corrosion resistance of Ni-P coatings in chloride-containing environments. In the present work, a Ni-P-TiO_2 composite coating was electroplated onto an AISI 430 steel substrate, and for the first time, the influence of electrodeposition current density on the microhardness, wear resistance, and corrosion performance of the coating was systematically investigated.

2. MATERIALS AND METHODS

In this work, AISI 430 stainless steels with dimensions of 10mm×10mm×2mm (chemical composition listed in Table 1) were employed as substrates.

TABLE 1. Chemical composition of AISI 430 stainless steels.

Element	P	S	Si	Mn	Cr	C	Fe
wt%	0.03	0.02	0.85	0.92	17.4	0.12	Bal

The steel surfaces were polished using silicon carbide abrasive papers with grit sizes of 400, 800, 1200, and 2500, followed by ultrasonic cleaning in acetone for 1 minute. To activate the surface, the substrates were immersed in a 10% sulfuric acid solution for 45 seconds. Prior to coating, electropolishing was performed in an 85 vol.% H_3PO_4 solution at a current density of 150 $mA.cm^{-2}$ for 2 minutes. The electrolyte composition and plating parameters for the Ni-P-TiO_2 coating electrodeposition are summarized in Table 2.

TABLE 2. Composition and bath conditions for the electroplating of Ni-P-TiO_2 coating.

Material	Concentration (g/L)
Nickel(II) chloride ($NiCl_2$)	40
Nickel(II) sulfate ($NiSO_4$)	280
Boric acid (H_3BO_3)	40
Sodium hypophosphite ($NaPO_2H_2$)	15
Titanium oxide (TiO_2)	40
SDS	0.3
Saccharin ($C_7H_5NO_3S_1$)	1
Current density	15, 25 and 35 $mA.cm^{-2}$
pH	3.5
Plating time	30 min
Plating temperature	60 °C

The schematic of the electroplating setup is illustrated in Figure 1. In the electrolyte bath, saccharin and sodium dodecyl sulfate (SDS) were employed as a grain-refining agent and a wetting agent, respectively. The bath pH was controlled by the addition of 3 M NaOH and 10% H_2SO_4 solutions. The surface morphology and chemical composition of the deposited coatings were characterized using a CamScan MV2300 scanning electron microscope (SEM) equipped with an energy-dispersive X-ray spectroscopy (EDS) system, while phase analysis was performed by X-ray diffraction (XRD). The average crystallite size of the coatings was estimated using Scherrer's equation (Meshram, 2022).

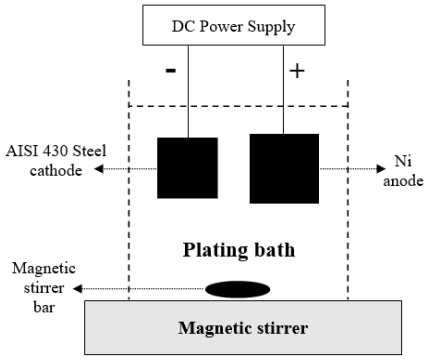

Figure 1. A schematic of setup used for Ni-P-TiO_2 coating electrodeposition.

The microhardness of the specimens was measured using a FURTHER-TECH CORP (Japan) FM700 microprocessor-based tester. Measurements were conducted on the cross-sections of all samples under a 50 g load with a dwell time of 10 s. Reported microhardness values represent the average of three individual tests. Wear performance was evaluated in accordance with ASTM G99. The pins used were carbon steel 5210 with a hardness of 64 RC. The wear test was carried out at a load of 5 N, a sliding velocity of 2.5 $m.s^{-1}$, and a total sliding distance of 1 m. The friction coefficient was calculated using CDT125 software. The worn path was investigated using SEM to study the wear mechanisms. Electrochemical behavior was assessed in a conventional three-electrode system comprising the sample (coated or uncoated) as the working electrode, a saturated calomel reference electrode (SCE), and a platinum counter electrode. All tests were carried out in 3.5 wt.% NaCl solution (Merck) at ambient temperature. Potential control and current response were recorded using an EG&G potentiostat (Model 263A). Potentiodynamic polarization experiments were performed at a potential sweep rate of 1 $mV.s^{-1}$ in both anodic and cathodic directions. Electrochemical impedance spectroscopy (EIS) was conducted at the corrosion potential (E_{corr}) in the frequency range of 10^{-2}-10^{5} Hz with an excitation amplitude of 5 mV for each sample. Polarization data were analyzed using CorrView software, and impedance spectra were fitted using ZView software.

3. RESULTS AND DISCUSSION

3.1. Influence of current density on microstructure of coating

Figure 2 presents the surface morphology of the Ni-P-TiO_2 composite coatings deposited at various current densities under a pH of 3.5 and a TiO_2 concentration of 40 $g.L^{-1}$. The coating obtained at 15 $mA.cm^{-2}$ exhibited a relatively smooth surface, although some spherical agglomerates were observed (Figure 2a). At 25 $mA.cm^{-2}$, the coating surface appeared non-uniform (Figure 2b), while the sample deposited at 35 $mA.cm^{-2}$ displayed a distinctly uneven and irregular morphology (Figure 2c).

Figure 3 illustrates the SEM micrograph of the composite coating produced at a current density of 15 $mA.cm^{-2}$, along with the corresponding elemental mapping of the surface. The mapping results confirm that TiO_2 nanoparticles are uniformly distributed within the Ni-P matrix without noticeable agglomeration. Table 3 presents the EDS analysis of Ni-P-TiO_2 composite coatings deposited at current densities of 15, 25, and 35 $mA.cm^{-2}$. It is evident that the maximum titanium incorporation, 12.58 wt.%, occurs at 15 $mA.cm^{-2}$. With increasing current density, the TiO_2 content in the coating progressively decreases, reaching its minimum value at 35 $mA.cm^{-2}$. According to the Celis model (Celis et al., 1987), the incorporation of particles into a metallic matrix occurs through a sequence of five stages: (i) formation of ionic clouds around the nanoparticles, (ii) transport of nanoparticles from the hydrodynamic layer to the cathode surface by convective currents, (iii) migration of the particles through the concentration layer via diffusion, (iv) passing through the electric double layer under the influence of electrophoretic forces, and (v) physical adsorption on the cathode surface followed by strong incorporation within the growing coating through reduction of surrounding metal ions.

TABLE 3. EDS analysis Ni-P-TiO_2 composite coating at the current density of 15, 25 and 35 $mA.cm^{-2}$

	Ni (wt%)	P (wt%)	Ti (wt%)	O (wt%)
i=15 ($mA.cm^{-2}$)	75.51	3.50	12.58	8.41
i=25 ($mA.cm^{-2}$)	80.31	4.20	9.28	6.21
i=35 ($mA.cm^{-2}$)	83.91	4.10	7.19	4.80

With increasing current density, the tendency for particles to reach and be adsorbed onto the cathode surface changes significantly. At higher current densities, the reduction of nickel ions becomes governed primarily by mass transfer, resulting in faster mobility of free nickel ions compared to those surrounding the nanoparticles. Consequently, the nickel ions near the particles have a reduced probability of reaching the cathode, while free ions preferentially deposit on the electrode surface. This mechanism decreases the extent of particle co-deposition as the current density rises. Furthermore, under very high current densities, the rapid movement of nickel ions hinders their precipitation on the particle surface, weakening particle adsorption at the cathode. These loosely attached particles may subsequently detach due to collisions, further reducing particle incorporation in the coating (Rudnik, 2024).

Additionally, elevated current densities enhance electrode polarization, which accelerates hydrogen evolution at the cathode surface. This effect diminishes particle incorporation, as reported by Elansezhian (Elansezhian et al., 2009). It is therefore evident that both current density and hydrogen evolution directly influence the coating's microstructure and the extent of particle reinforcement within the metal matrix composite (Beltowska-Lehman et al., 2012; Ogihara et al., 2012).

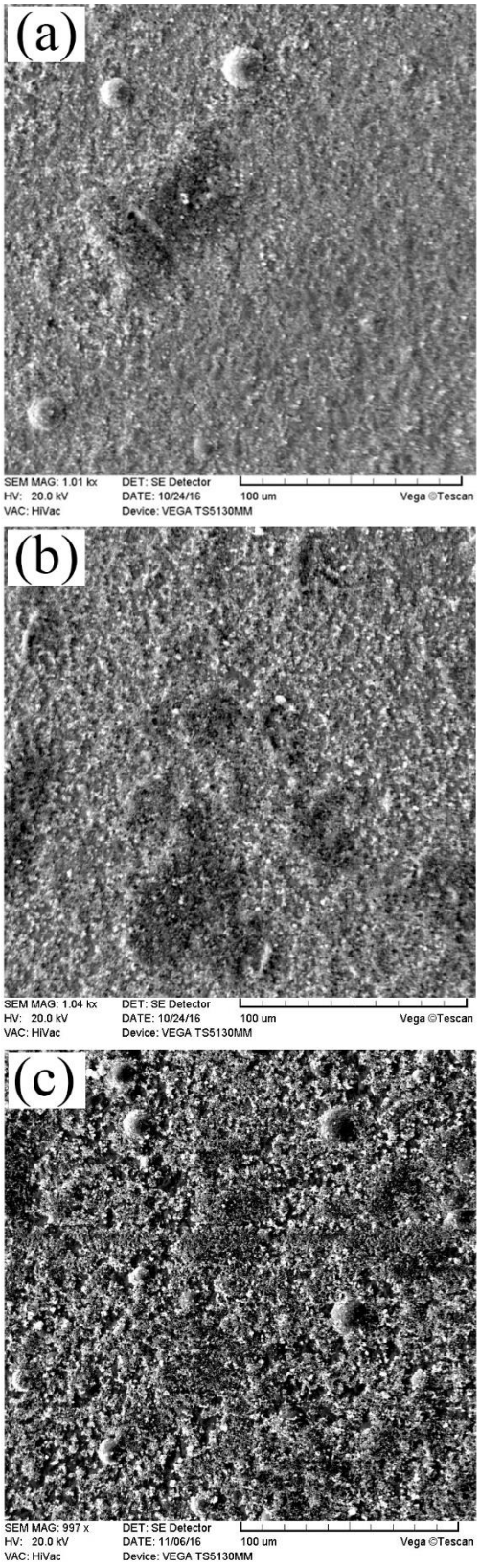

Figure 2. SEM image of surface morphology of Ni-P-TiO_2 composite coating at different current densities of: (a) 15, (b) 25 and (c) 35 $mA.cm^{-2}$.

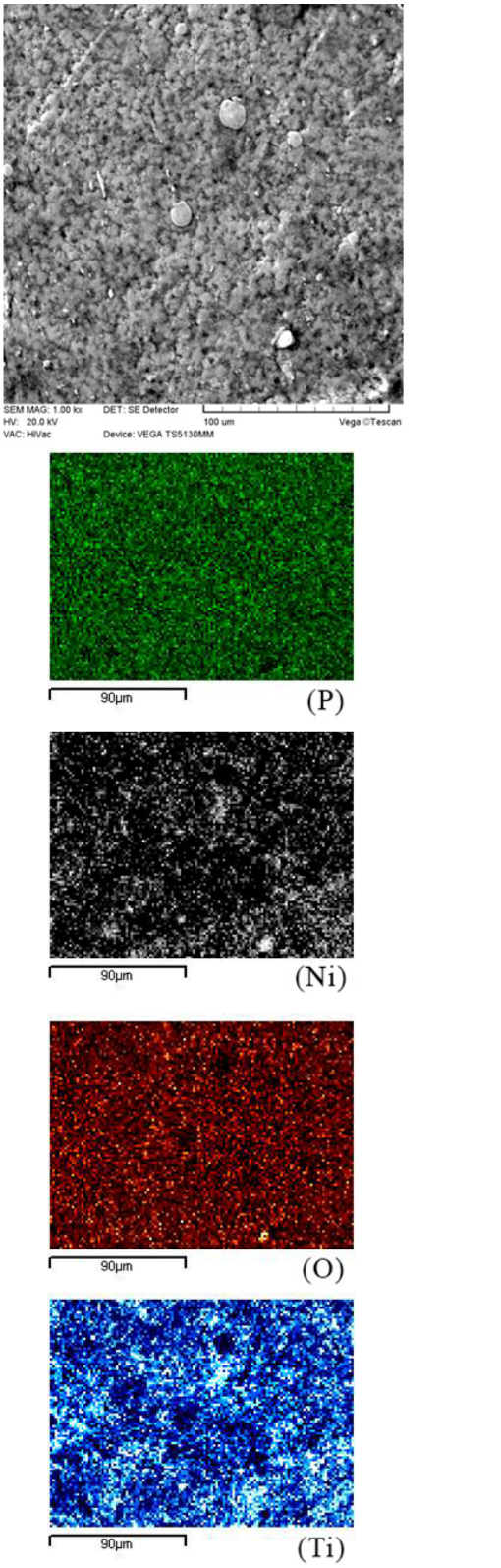

Figure 3. Distribution of Ni, P, Ti, and O alloying elements in Ni-P-TiO_2 composite coating at a current density of 15 $mA.cm^{-2}$.

Sasi et al. (2015) studied the influence of current density on the properties of Ni-Al_2O_3 coatings and demonstrated that higher current densities improved hardness and wear resistance of the coating.

The evolution of hydrogen during electrodeposition plays a crucial role in the development of residual stress. The dependence of residual stress in Ni-P coatings on current density can be explained by the accelerated deposition of atoms on the substrate surface at higher current densities, which enhances lattice mismatch and consequently increases residual stress. In addition, stress generation within the coating is strongly linked to the co-deposition of metal and hydrogen species during the plating process (Wang et al., 2012). The incorporation of TiO_2 particles further influences this behavior, as these particles can adsorb hydrogen ions near the cathode. This adsorption not only reduces the likelihood of hydrogen evolution but also limits the reduction of phosphorous acid to elemental phosphorus, subsequently decreasing the phosphorus concentration in the deposit while contributing to increased hardness. Nevertheless, the greater incorporation of hydrogen elevates residual stress levels, partially offsetting the hardness improvement (Gadhari & Sahoo, 2015). The voltage-time profile of the electroplating process is presented in Figure 4. For all applied current densities, the electrodeposition voltage rises progressively with deposition time, attributed to the increase in solution resistance (Reedijk & Poeppelmeier, 2023).

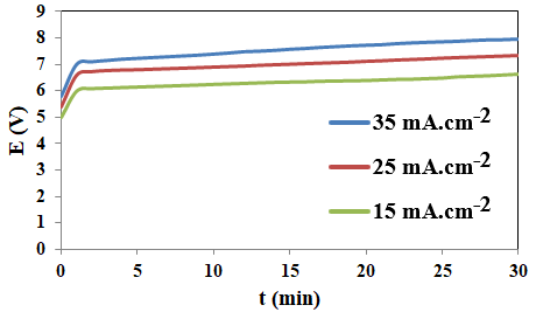

Figure 4. Voltage profile during the electrochemical deposition at different current densities.

At elevated current densities, increased evolution of hydrogen bubbles occurs on the cathode surface (reaction (1)), leading to a reduction in current efficiency and, consequently, a decreased deposition rate. This behavior is consistent with the observed changes in surface morphology at different current densities (Figure 2). Moreover, prolonging the electroplating time promotes unwanted reactions (reaction (2)), which in turn cause the electrolyte to become darker and less transparent (Ananth, 1997).

$$2H^+ + 2e^- \rightarrow H_2 \quad (1)$$

$$2H_2O + 2e^- \rightarrow H_2 + 2OH^- \quad (2)$$

In aqueous electrolytes containing $NiSO_4$, Ni^{2+} can exist in unstable complex forms such as $[Ni(H_2O)_6]^{2+}$, $[Ni(NH_3)_x]^{2+}$ (x = 1-6), and $[Ni(H_2O)_{6-n}(NH_3)_n]^{2+}$. It is also proposed that Ni^{2+} reduction can occur through the following mechanism (reactions (3) and (4)) in the presence of NH_3 (Bahramian et al., 2018; Lelevic & Walsh, 2019; Low & Walsh, 2015; Zhang et al., 2019).

$$[(Ni(H_2O)_{6-n}(NH_3)_n]^{2+} + xH_2O \rightarrow [(Ni(H_2O)_{6-n+x}]^{2+} + nNH_3 \quad (3)$$

$$[(Ni(H_2O)_{6-n+x}]^{2+} + 2e^- \rightarrow Ni + (6 - n + x)H_2O \quad (4)$$

At the initial stages of deposition, Ni^{2+} predominantly exists as $[Ni(H_2O)_6]^{2+}$. With prolonged deposition, however, it mainly transforms into $[Ni(H_2O)_{6-n}(NH_3)_n]^{2+}$ (Lelevic & Walsh, 2019; Low & Walsh, 2015; Zhang et al., 2019). Therefore, at short deposition times, the formation of proper complexes enhances Ni reduction, thereby improving current efficiency. It should be noted that at short deposition times, Ni ions are largely hydrated, and the solution exhibits relatively low resistance (Zhang et al., 2019). In contrast, at long deposition times, the formation of Ni hydroxide $[Ni(OH)_2]$ leads to solution turbidity, reduced current efficiency, and increased solution resistance, all of which negatively affect the electrodeposition of Ni-P-TiO_2.
Figure 5 illustrates the phosphorus content incorporated into the coating as a function of the applied current density. An increase in current density from 15 to 25 mA.cm^{-2} leads to a rise in phosphorus deposition, reaching approximately 4.2 wt.%. With further increase in current density up to 35 mA.cm^{-2}, no significant variation is observed. Each value represents the average of three independent measurements, while the error bars indicate the standard error of the mean.

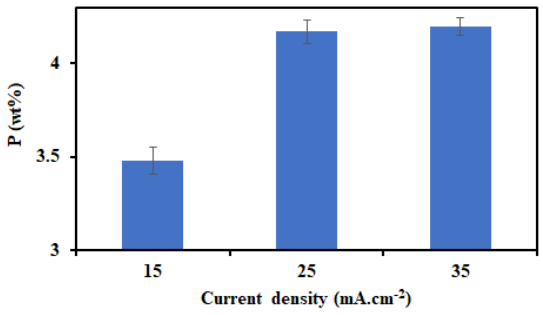

Figure 5. Influence of current density on the deposition value of P.

The influence of current density on phosphorus incorporation into the coating can be explained by the following reaction:

$$H_3PO_3 + 3H^+ + 3e^- \rightarrow P(s) + 3H_2O \quad (5)$$

As indicated by reaction (5), which involves the direct reduction of phosphorus from phosphoric acid, the formation of phosphorus requires the availability of hydrogen ions. An increase in current density

consequently enhances the phosphorus deposition rate until saturation is attained (Elansezhian et al., 2009).

Figure 6 presents the XRD results of the Ni-P-TiO_2 composite coating at different current densities. The diffraction peaks confirm the presence of Ni, TiO_2, and Ni_8P_3 phases. The angles of the main peaks and the associated diffraction planes are listed in Table 4. Based on the XRD results, particularly the broadening observed around the 2θ= 45° peak, the coating can be characterized as nanocrystalline with an ultrafine crystal structure (Low & Walsh, 2015). The X-ray diffraction pattern reveals a broad peak along with a low-intensity intermetallic peak superimposed on the Ni-amorphous peak. This indicates that, despite the relatively low phosphorus content (2.4-5.3 wt.%, i.e., below 5 wt.%), the coating exhibits a mixed

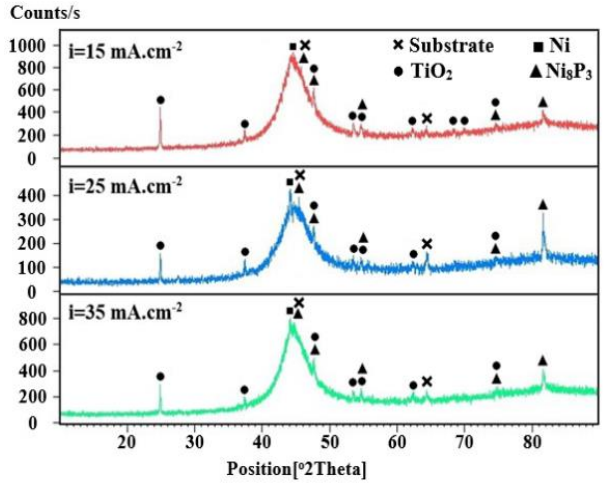

Figure 6. X-ray diffraction patterns of the samples coated at different pHs.

TABLE 4. The position and the diffraction planes observed in XRD pattern of the coatings.

Phase	Position (2θ)	Planes	JCPDS No.
Ni	44.02	(1 1 1)	04-0850
Substrate (Fe)	44.68	(1 1 0)	87-0721
	64.86	(2 0 0)	
Titanium oxide (TiO_2)	24.98	(1 0 1)	84-1286
	37.54	(0 0 4)	
	47.72	(2 0 0)	
	53.88	(1 0 5)	
	54.84	(2 1 1)	
	62.42	(2 0 4)	
	68.54	(1 1 6)	
	70.02	(2 2 0)	
	74.94	(2 1 5)	
Ni_8P_3	44.68	(2 1 7)	78-1183
	47.72	(3 0 0)	
	53.88	(1 2 14)	
	74.94	(0 0 30)	
	81.33	(2 3 14)	

Amorphous/nanocrystalline structure, similar to that typically observed in Ni-P alloys with phosphorus contents ranging from 0 to 9 wt.%. Generally, amorphous structures in Ni-P alloys become more pronounced as the phosphorus concentration increases; however, the microstructure is also strongly influenced by the deposition method. For instance, in electroplated coatings, amorphous phases may form even at comparatively lower phosphorus levels (Ogihara et al., 2012). Furthermore, the addition of saccharin decreases phosphorus incorporation into the nickel matrix while simultaneously promoting the formation of an amorphous phase even at low phosphorus concentrations (Ogihara et al., 2012). The presence of such amorphous phases in the coating structure has been reported to enhance corrosion resistance (Ahmadkhaniha & Zanella, 2019). The crystallite size of Ni-P-TiO_2 composite coatings at current densities of 15, 25, and 35 $mA.cm^{-2}$ was approximately 37, 42, and 49 nm, respectively. As the current density increases, the mobility of both particles and ions is significantly enhanced. Based on Guglielmi's theory (Guglielmi, 1972), particles deposited on the surface can rapidly desorb due to their high activity, which decreases the overall particle incorporation. This reduction in effective nucleation sites favors the growth of existing crystallites, leading to an increase in crystallite size. When insufficient nucleation sites are available on the substrate, growth processes dominate over nucleation, causing incoming particles to preferentially absorb onto pre-existing nuclei rather than initiating new ones. Consequently, higher current density accelerates crystal growth, ultimately promoting larger crystallite sizes, as the more energetic particles are more mobile and can coalesce with adjacent nuclei (Ebrahimifar & Zandrahimi, 2017).

Supporting these findings, a study investigating the effect of current density on the crystallite size of Ni-P coatings. Uhm (Uhm et al., 2015) reported that increasing the current density up to 12 $mA.cm^{-2}$ leads to a reduction in crystallite size, primarily because the nucleation rate exceeds the growth rate. However, when the current density rises beyond 15 $mA.cm^{-2}$, the coating density decreases and the crystallite size increases. This effect has been attributed to enhanced hydrogen evolution at the cathode surface, which aligns with the observations above. Under such conditions, variations in surface energy and growth mechanisms are considered responsible for the enlargement of crystallite size with increasing current density (Rashidi & Amadeh, 2008). Furthermore, the incorporation of TiO_2 particles within the coating has been shown to restrict crystal growth, thereby reducing crystallite size (Wasekar et al., 2016). Consequently, lower current densities, which facilitate higher incorporation of TiO_2 particles, result in smaller crystallite sizes.

3.2. Influence of current density on mechanical properties

The microhardness of the uncoated sample and Ni-P-TiO_2-coated samples at current densities of 15, 25, and 35 $mA.cm^{-2}$ was 215.8, 598.7, 571, and 565.2 HV, respectively. Each value represents the mean of three measurements, and the associated error bars correspond to the standard error of the mean. As illustrated, increasing the current density from 15 to 35 $mA.cm^{-2}$ leads to a reduction in microhardness, with the maximum hardness recorded at 15 $mA.cm^{-2}$. At 35 $mA.cm^{-2}$, both TiO_2 incorporation into the coating and hardness reach their minimum levels. This observation indicates that higher current density reduces TiO_2 particle deposition, which in turn diminishes hardness. Moreover, increasing current density results in larger crystallite sizes, and according to the Hall-Petch relationship, an increase in crystallite size decreases hardness. Based on the models proposed by Winand (Winand, 1994) and Dini (Dini, 1993), an increase in current density is generally expected to reduce the crystallite size of electrodeposited coatings. However, several studies on direct current (DC) electrodeposition of nickel from different electrolytic baths have reported the opposite trend, where crystallite size increases with higher current density (Cziráki et al., 1994; Ebrahimi & Ahmed, 2003).

According to Cziráki et al. (1994), this enlargement of crystallites at relatively high current densities arises from the depletion of Ni^{2+} ions at the deposit-electrolyte interface. Ebrahimi & Ahmed (2003) further attributed this phenomenon to the enhanced co-deposition of hydrogen at the cathode surface. The presence of hydrogen modifies surface energy and alters growth mechanisms, ultimately promoting crystallite coarsening with increasing current density. The weight loss of the uncoated sample and Ni-P-TiO_2-coated samples at current densities of 15, 25, and 35 $mA.cm^{-2}$ (pH = 3.5, TiO_2 = 40 $g.L^{-1}$) was 1.2, 0.2, 0.35, and 0.4 mg, respectively. Among these, the coating produced at 15 $mA.cm^{-2}$ exhibited the lowest weight loss, while increasing current density corresponded to higher material loss. During wear, TiO_2 particles may detach from the coating surface, thereby reducing the effective contact area between the pins and the composite surface. Acting as solid lubricants (Mohanty et al., 2002), these particles enhance wear resistance; consequently, a reduction in TiO_2 incorporation diminishes this effect. Furthermore, as current density increases, hardness decreases, and according to Archard's law (Archard, 1953), this drop in hardness further reduces wear resistance. It is also noteworthy that the coefficient of friction plays an important role in the wear performance of coatings (Neale & Gee, 2001).

Figure 7 illustrates the influence of current density on the friction coefficient at pH = 3.5 with a TiO_2 concentration of 40 $g.L^{-1}$. The substrate exhibits the highest friction coefficient, whereas the composite coatings demonstrate significantly lower values. At a current density of 15 $mA.cm^{-2}$, the composite coating attains its minimum friction coefficient; however, as the current density increases to 35 $mA.cm^{-2}$, the coefficient gradually rises. This behavior can be attributed to the reduced incorporation of particles at higher current densities, which diminishes their solid lubrication effect and consequently leads to an increase in friction (Saravanan et al., 2020).

Figure 8 presents SEM micrographs of the worn surfaces of composite coatings produced at a TiO_2 concentration of 40 $g.L^{-1}$ under varying current densities. At 15 $mA.cm^{-2}$ (Figure 8a), the worn path exhibits a comparatively smoother morphology with a narrower width relative to coatings deposited at higher current densities. In contrast, at 35 $mA.cm^{-2}$, the worn surface displays the greatest depth and width (Figure 8c). Furthermore, signs of plastic deformation and surface degradation are evident along the worn path in Figures 8b and 8c. These observations indicate that, with increasing current density, the decline in TiO_2 particle incorporation and coating hardness intensifies wear severity, primarily through adhesion and delamination mechanisms.

3.3. Influence of current density on corrosion behavior of coating

Figure 9 shows the potentiodynamic polarization curves for coated specimens at current densities of 15, 25, and 35 $mA.cm^{-2}$ in 3.5% NaCl solution.

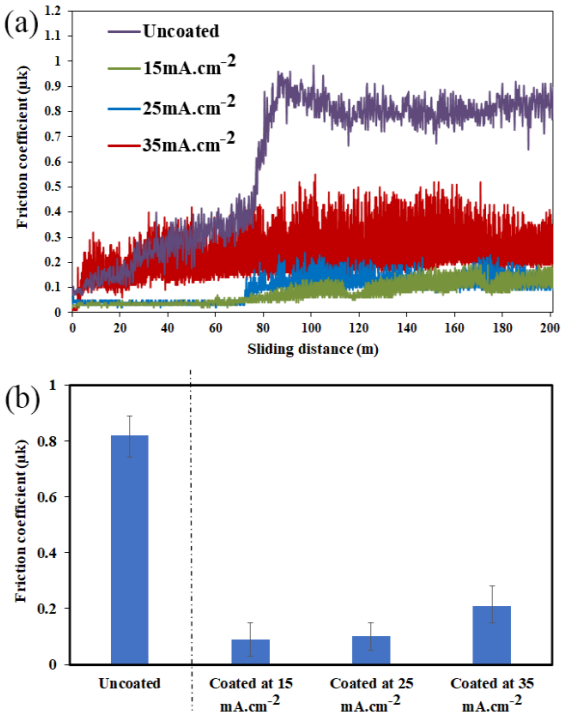

Figure 7. (a) Changes of friction coefficient versus distance and (b) mean values of friction coefficient for different samples after sliding distance of 200m.

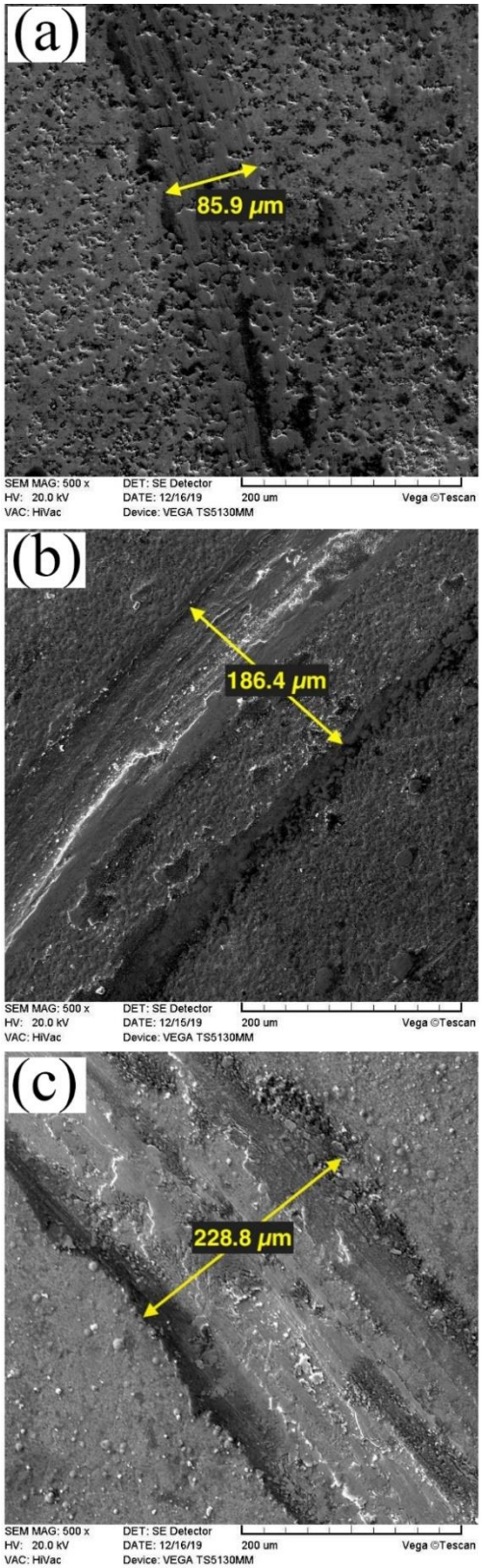

Figure 8. Wear path of coatings created at current density of: (a) 15, (b) 25 and (c) 35 mA.cm^{-2}.

The extrapolation of Tafel polarization curves was performed using Corrview software, and the corresponding results are summarized in Table 5. Polarization resistance (R_p) was calculated based on the Stern-Geary equation (Liu et al., 2009), where R_p denotes the polarization resistance, β_a and β_c represent the anodic and cathodic Tafel slopes, respectively, and icorr corresponds to the corrosion current density. The results indicate that increasing the current density of the electroplating bath from 15 to 35 mA.cm^{-2} results in a higher corrosion current density of the composite coating. Additionally, Figures 10a, 10b, and 10c present the Nyquist, Bode, and Bode-phase plots, respectively, for all samples immersed in 3.5 wt.% NaCl solution, recorded over a frequency range of 0.01 to 10 kHz. The deviation of the Nyquist plots from an ideal semicircle reflects the surface roughness and heterogeneity of the coatings during the corrosion process (Cai et al., 2011).

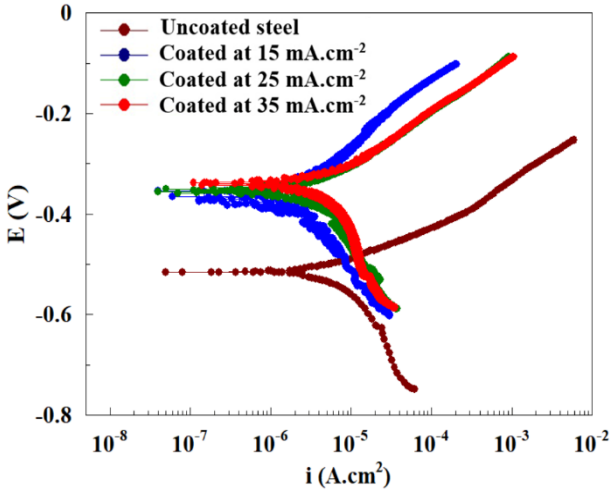

Figure 9. Polarization diagram of the different samples.

TABLE 5. Data obtained from the polarization curve at current densities of 15, 25 and 35 mA.cm^{-2}.

Sample	blank	Coated at i=15 (mA.cm^{-2})	Coated at i=25 (mA.cm^{-2})	Coated at i=35 (mA.cm^{-2})
E_{corr} (mV)	-0.51	-0.37	-0.35	-0.34
i_{corr} (μA.cm^{-2})	2.65	1.27	1.72	2.31
β_c (mV.dec^{-1})	82.83	82.35	59.12	78.82
β_a (mV.dec^{-1})	54.83	63.56	57.14	56.69
R_p (Ω.cm^2)	5403	12217	7334	6193

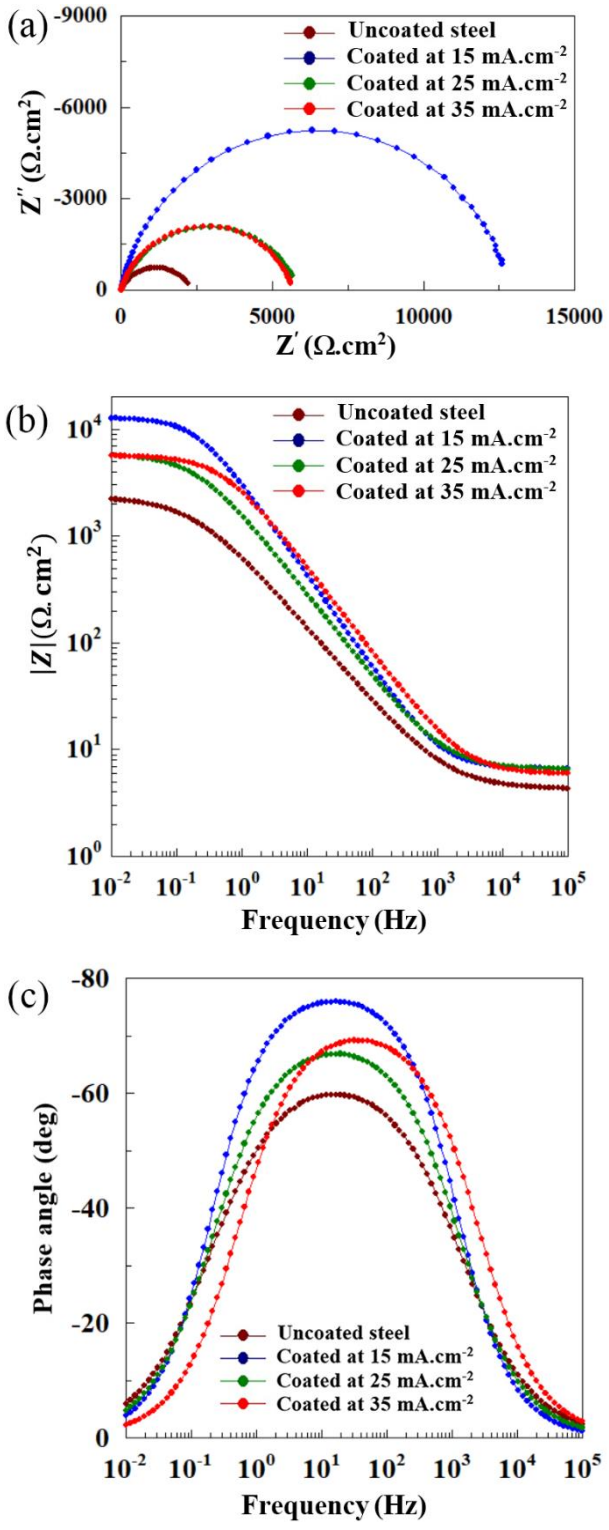

Figure 10. (a) Nyquist and (b) Bode and (c) Bode-phase diagrams of the different samples.

The equivalent electrical circuits simulated using ZView software for the investigated samples are shown in Figure 11. In these models, R_s represents the solution resistance, R_{ct} and R_{coat} denote the charge transfer resistance and coating resistance, respectively, and CPE corresponds to the constant phase element. The electrochemical parameters extracted from the impedance spectra are summarized in Table 6. The data indicate that R_{ct} decreases with increasing current density, suggesting that the coating deposited at 15 mA.cm^{-2} exhibits superior corrosion resistance compared to those produced at higher current densities. Furthermore, the coating deposited at 15 mA.cm^{-2} displays a lower CPE-T_{coat} value relative to the other coatings, indicating reduced porosity and consequently more restricted electrolyte penetration (Salahinejad, et al., 2013; Zhang et al., 2010).

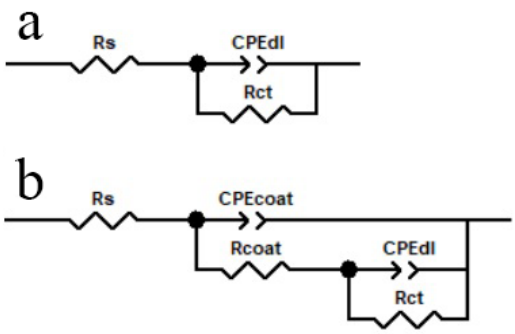

Figure 11. Equivalent electrical circuit used for (a) uncoated and (b) coated samples.

TABLE 6. Electrochemical data derived from impedance curves of uncoated and coated samples.

Sample	blank	Coated at i=15 (mA.cm^{-2})	Coated at i=25 (mA.cm^{-2})	Coated at i=35 (mA.cm^{-2})
R_s (Ω.cm^2)	4.24	6.64	6.48	5.87
CPE-T_{coat} (Ω^{-1}.cm^{-2}.S^n)	-	5.9E-5	1.35E-4	6.7E-5
CPE-P_{coat} (Ω^{-1}.cm^{-2}.S^n)	-	0.89	0.78	0.81
R_{ccoat} (Ω.cm^2)	-	11710	5280	5530
CPE-T_{dl} (Ω^{-1}.cm^{-2}.S^n)	3.72E-4	9E-4	1E-3	7E-3
CPE-P_{dl} (Ω^{-1}.cm^{-2}.S^n)	0.71	0.92	0.87	0.83
R_{ct} (Ω.cm^2)	2332	1053	650	215

The incorporation of reinforcing particles enhances the corrosion resistance of Ni-P composite coatings. In particular, the addition of TiO_2 particles modifies the coating microstructure and refines crystallite size, thereby improving protective performance (Zhang et al., 2007). These non-conductive and chemically inert particles reduce the effective surface area exposed to the corrosive medium and help fill surface defects such as cavities and microcracks (Zhang et al., 2010). Their

presence within the Ni-P matrix also decreases the density of electrochemically active sites, suppressing anodic dissolution of the metallic matrix and thereby increasing the overall corrosion resistance of the composite coatings.

In addition, TiO_2 particles extend the corrosion pathway, introducing a more indirect diffusion route that hinders the penetration of corrosive agents toward the substrate, further enhancing corrosion resistance (Zhang et al., 2007). Consequently, the higher incorporation of TiO_2 particles in the coating deposited at 15 $mA.cm^{-2}$ contributes significantly to its superior corrosion resistance compared with coatings formed at higher current densities. In contrast, surface cavities and localized substrate exposure in coatings produced at elevated current densities accelerate corrosion, resulting in higher rates relative to samples prepared at 15 $mA.cm^{-2}$.

4. CONCLUSION(S)

Ni-P-TiO_2 composite coatings were electrodeposited on AISI 430 stainless steel, and the influence of current density on their microstructure, mechanical properties, and corrosion behavior was systematically investigated. The main findings are summarized as follows:

1. Increasing the current density up to 35 $mA.cm^{-2}$ decreased TiO_2 particle incorporation, promoted cavity formation within the coating, and enhanced phosphorus deposition.
2. Crystallite size increased with current density, while maximum microhardness was achieved at 15 $mA.cm^{-2}$.
3. The coating deposited at 15 $mA.cm^{-2}$ exhibited the best wear resistance and corrosion protection compared with coatings formed at higher current densities.

ACKNOWLEDGEMENT

I would like to express my gratitude to my late professor, Morteza Zandrahimi, for sharing his knowledge with me throughout this research. His instruction and assistance considerably aided me in becoming an independent problem solver. His memory will always be with me, and I sincerely offer my condolences to his loving family.

REFRENCES

1. Ahmadkhaniha, D., & Zanella, C. (2019). The effects of additives, particles load and current density on codeposition of SiC particles in NiP nanocomposite coatings. *Coatings*, *9*(9). https://doi.org/10.3390/coatings9090554
2. Ananth, M. V. (1997). Corrosion studies on electrodeposited nickel-manganese coatings. *Transactions of the Institute of Metal Finishing*, *75*(6). https://doi.org/10.1080/00202967.1997.11871179
3. Archard, J. F. (1953). Contact and rubbing of flat surfaces. *Journal of Applied Physics*, *24*(8). https://doi.org/10.1063/1.1721448
4. Bahramian, A., Eyraud, M., Vacandio, F., & Knauth, P. (2018). Improving the corrosion properties of amorphous Ni-P thin films using different additives. *Surface and Coatings Technology*, *345*. https://doi.org/10.1016/j.surfcoat.2018.03.075
5. Beltowska-Lehman, E., Bigos, A., Indyka, P., & Kot, M. (2012). Electrodeposition and characterisation of nanocrystalline Ni-Mo coatings. *Surface and Coatings Technology*, *211*. https://doi.org/10.1016/j.surfcoat.2011.10.011
6. Cai, C., Zhu, X. B., Zheng, G. Q., Yuan, Y. N., Huang, X. Q., Cao, F. H., Yang, J. F., & Zhang, B. (2011). Electrodeposition and characterization of nano-structured Ni-SiC composite films. *Surface and Coatings Technology*, *205*(11). https://doi.org/10.1016/j.surfcoat.2010.12.002
7. Celis, J. P., Roos, J. R., & Buelens, C. (1987). A mathematical model for the electrolytic codeposition of particles with a metallic matrix. *Journal of The Electrochemical Society*, *134*(6). https://doi.org/10.1149/1.2100680
8. Chen, W., Gao, W., & He, Y. (2010). A novel electroless plating of Ni-P-TiO_2 nano-composite coatings. *Surface and Coatings Technology*, *204*(15). https://doi.org/10.1016/j.surfcoat.2010.01.032
9. Chou, M. C., Ger, M. D., Ke, S. T., Huang, Y. R., & Wu, S. T. (2005). The Ni-P-SiC composite produced by electro-codeposition. *Materials Chemistry and Physics*, *92*(1). https://doi.org/10.1016/j.matchemphys.2005.01.021
10. Cziráki, A., Fogarassy, B., Gerőcs, I., Tóth-Kádár, E., & Bakonyi, I. (1994). Microstructure and growth of electrodeposited nanocrystalline nickel foils. *Journal of Materials Science*, *29*(18). https://doi.org/10.1007/BF00356522
11. Dini, J. W. (1993). Electrodepositlon: the materials science of coatings and substrates. In *British Corrosion Journal* (Vol. 28). https://cir.nii.ac.jp/crid/1571417124775217920
12. Ebrahimi, F., & Ahmed, Z. (2003). The effect of current density on properties of electrodeposited nanocrystalline nickel. *Journal of Applied Electrochemistry*, *33*(8). https://doi.org/10.1023/A:1025049802635
13. Ebrahimifar, H., & Zandrahimi, M. (2017). Influence of electrodeposition parameters on the characteristics of Mn-Co coatings on Crofer 22 APU ferritic stainless steel. *Bulletin of Materials Science*, *40*(6). https://doi.org/10.1007/s12034-017-1473-2
14. Elansezhian, R., Ramamoorthy, B., & Nair, P. K. (2009). The influence of SDS and CTAB surfactants on the surface morphology and surface topography of electroless Ni-P deposits. *Journal of Materials Processing Technology*, *209*(1). https://doi.org/10.1016/j.jmatprotec.2008.01.057
15. Fukunaga, A., & Ueda, S. (2024). Pulse electrodeposition of Ni-P alloy coatings from Watts baths: P content, current efficiency, and internal stress. *Electrochimica Acta*, *502*, 144839. https://doi.org/10.1016/J.ELECTACTA.2024.144839
16. Gadhari, P., & Sahoo, P. (2015). Optimization of coating process parameters to improve microhardness of Ni-P-TiO_2 composite coatings. *Materials Today: Proceedings*, *2*(4-5). https://doi.org/10.1016/j.matpr.2015.07.303
17. Guglielmi, N. (1972). Kinetics of the deposition of inert particles from electrolytic baths. *Journal of The Electrochemical Society*, *119*(8). https://doi.org/10.1149/1.2404383
18. Hansal, W. E., Sandulache, G., Mann, R., & Leisner, P. (2013). Pulse-electrodeposited NiP-SiC composite coatings. *Electrochemical Acta*, *114*. https://doi.org/10.1016/j.electacta.2013.08.182

19. Karthik, R., Mani, R., & Manikandan, P. (2020). Tribological studies of Ni-SiC and Ni-Al_2O_3 composite coatings by pulsed electrodeposition. *Materials Today: Proceedings*, *37*(Part 2). https://doi.org/10.1016/j.matpr.2020.05.717

20. Lekmine, F., Naoun, M., Gana, A., & Ben Temam, H. (2022). Structural, mechanical and corrosion behavior of Ni-P-TiO_2 composite coatings: effect of current density. *Journal of Nano- and Electronic Physics*, *14*(1). https://doi.org/10.21272/jnep.14(1).01009

21. Lelevic, A., & Walsh, F. C. (2019). Electrodeposition of NiP composite coatings: A review. *Surface and Coatings Technology*, *378*, 124803. https:/doi.org/10.1016/j.surfcoat.2019.07.027

22. Liu, X., Xiong, J., Lv, Y., & Zuo, Y. (2009). Study on corrosion electrochemical behavior of several different coating systems by EIS. *Progress in Organic Coatings*, *64*(4). https://doi.org/10.1016/j.porgcoat.2008.08.012

23. Low, C. T. J., & Walsh, F. C. (2015). Multifunctional nanostructured metallic coatings by electrodeposition. In *Multifunctional Materials for Tribological Applications*. https://doi.org/10.1201/b18311-9

24. Ma, C., Wang, C., Xia, F., Wang, Q., Yan, P., & Zhang, Y. (2024). Microstructure, wear and corrosion resistances of Ni-ZrO_2-CeO_2 nanocoatings. *Ceramics International*, *50*(12). https://doi.org/10.1016/j.ceramint.2024.03.157

25. Meshram, A. P., Gupta, A., & Srivastava, C. (2022). Effect of electrodeposition temperature on texture, strain, grain boundary constitution and corrosion behavior of Ni-P coatings with low phosphorous content. *Materialia, 22.*. https://doi.org/10.1016/j.mtla.2022.101413

26. Mohanty, U. S., Tripathy, B. C., Singh, P., & Das, S. C. (2002). Effect of Cr^{3+} on the electrodeposition of nickel from acidic sulfate solutions. *Minerals Engineering*, *15*(7). https://doi.org/10.1016/S0892-6875(02)00076-6

27. Mohsenifar, F., Ebrahimifar, H., & Irannejad, A. (2024). Investigation of Electrodeposited Mn-Co-Y_2O_3 Coating on Crofer 22 APU for the SOFC Interconnect Application. *Protection of Metals and Physical Chemistry of Surfaces*, *60*(6), 1033-1049. https://doi.org/10.1134/S2070205124702496

28. Neale, M. J., & Gee, M. (2001). Chapter 2 - Industrial wear problems. In M. J. Neale & M. Gee (Eds.), *A Guide to Wear Problems and Testing for Industry* (pp. 3-III). William Andrew Publishing. https:/doi.org/10.1016/B978-081551471-8.50002-5

29. Ogihara, H., Safuan, M., & Saji, T. (2012). Effect of electrodeposition conditions on hardness of Ni-B/diamond composite films. *Surface and Coatings Technology*, *212*. https://doi.org/10.1016/j.surfcoat.2012.09.045

30. Rai, P. K., & Gupta, A. (2021). Investigation of surface characteristics and effect of electrodeposition parameters on nickel-based composite coating. *Materials Today: Proceedings*, *44*. https://doi.org/10.1016/j.matpr.2020.11.182

31. Rashidi, A. M., & Amadeh, A. (2008). The effect of current density on the crystallite size of electrodeposited nanocrystalline nickel coatings. *Surface and Coatings Technology*, *202*(16). https://doi.org/10.1016/j.surfcoat.2008.01.018

32. Reedijk, J., & Poeppelmeier, K. R. (2023). Comprehensive Inorganic Chemistry III, Third Edition. In *Comprehensive Inorganic Chemistry III, Third Edition* (Vols. 1-10).

33. Rudnik, E. (2024). Black nickel coatings: from plating techniques to applications. *Coatings*, *14*(12). https://doi.org/10.3390/coatings14121588

34. Sadeghi, A. (2016). *Microstructure Evolution and Strengthening Mechanism in Ni-based Composite Coatings* [Doctorial thesis, Technische Universität Chemnitz]. https://nbn-resolving.org/urn:nbn:de:bsz:ch1-qucosa-211837

35. Salahinejad, E., Hadianfard, M. J., Macdonald, D. D., Sharifi, S., Mozafari, M., Walker, K. J., Tahmasbi Rad, A., Madihally, S. V., Vashaee, D., & Tayebi, L. (2013). Surface modification of stainless steel orthopedic implants by sol-gel $ZrTiO_4$ and $ZrTiO_4$-PMMA coatings. *Journal of Biomedical Nanotechnology*, *9*(8). https://doi.org/10.1166/jbn.2013.1619

36. Saravanan, I., Elayaperumal, A., Devaraju, A., Karthikeyan, M., & Raji, A. (2020). Wear behaviour of electroless Ni-P and Ni-P-TiO_2 composite coatings on En8 steel. *Materials Today: Proceedings*, *22*, 1135–1139. https:/doi.org/10.1016/j.matpr.2019.12.007

37. Sasi, A., Mondal, M., Dayal, S., & Kumar, S. (2015). Electro deposition of nickel-alumina composite coating. *Materials Today: Proceedings*, *2*(4-5). https://doi.org/10.1016/j.matpr.2015.07.292

38. Shozib, I. A., Ahmad, A., Rahaman, M. S. A., Abdul-Rani, A. M., Alam, M. A., Beheshti, M., & Taufiqurrahman, I. (2021). Modelling and optimization of microhardness of electroless Ni-P-TiO_2 composite coating based on machine learning approaches and RSM. *Journal of Materials Research and Technology*, *12*. https://doi.org/10.1016/j.jmrt.2021.03.063

39. Sun, J., Tang, H., Wang, C., Han, Z., & Li, S. (2022). Effects of alloying elements and microstructure on stainless steel corrosion: A review. In *Steel Research International* (Vol. 93, Issue 5). https://doi.org/10.1002/srin.202100450

40. Uhm, Y. R., Park, K. Y., & Choi, S. J. (2015). The effects of current density and saccharin addition on the crystallite size of electroplated nickel. *Research on Chemical Intermediates*, *41*(7). https://doi.org/10.1007/s11164-013-1518-0

41. Wang, J., Xu, R., & Zhang, Y. (2012). Study on characteristics of Ni-W-B composites containing CeO_2 nano-particles prepared by pulse electrodeposition. *Journal of Rare Earths*, *30*(1). https://doi.org/10.1016/S1002-0721(10)60636-9

42. Wasekar, N. P., Haridoss, P., Seshadri, S. K., & Sundararajan, G. (2016). Influence of mode of electrodeposition, current density and saccharin on the microstructure and hardness of electrodeposited nanocrystalline nickel coatings. *Surface and Coatings Technology*, *291*. https://doi.org/10.1016/j.surfcoat.2016.02.024

43. Winand, R. (1994). Electrodeposition of metals and alloys-new results and perspectives. *Electrochimica Acta*, *39*(8-9). https://doi.org/10.1016/0013-4686(94)E0023-S

44. Yongfeng, L., Limin, Z., Zhankui, W., Lijie, M., Jianxiu, S., Chang, L., & MingChao, J. (2017). Ni-P-TiO_2 nanoparticle composite formed by chemical plating: deposition rate and corrosion resistance. *International Journal of Electrochemical Science*, *12*(4). https://doi.org/10.20964/2017.04.41

45. Zhang, H., Wang, J., Chen, S., Wang, H., He, Y., & Ma, C. (2021). Ni-SiC composite coatings with improved wear and corrosion resistance synthesized via ultrasonic electrodeposition. *Ceramics International*, *47*(7). https://doi.org/10.1016/j.ceramint.2020.12.076

46. Zhang, S., Li, Q., Yang, X., Zhong, X., Dai, Y., & Luo, F. (2010). Corrosion resistance of AZ91D magnesium alloy with electroless plating pretreatment and Ni-TiO_2 composite coating. *Materials Characterization*, *61*(3). https://doi.org/10.1016/j.matchar.2009.10.006

47. Zhang, W., Cao, D., Qiao, Y., He, Z., Wang, Y., Li, X., & Gao, W. (2019). Microstructure and properties of duplex Ni-P-TiO_2/Ni-P nanocomposite coatings. *Materials Research*, *22*. https://doi.org/10.1590/1980-5373-MR-2018-0748

48. Zhang, X., Wang, F., & Du, Y. (2007). Effect of nano-sized titanium powder addition on corrosion performance of epoxy coatings. *Surface and Coatings Technology*, *201*(16-17). https://doi.org/10.1016/j.surfcoat.2007.01.042